PERGAMON

International Journal of Solids and Structures 40 (2003) 6859–6876

INTERNATIONAL JOURNAL OF SOLIDS and STRUCTURES

www.elsevier.com/locate/ijsolstr

Exact solutions for magneto-electro-elastic laminates in cylindrical bending

E. Pan [a,*], P.R. Heyliger [b]

[a] Department of Civil Engineering, University of Akron, Akron, OH 44325-3905, USA
[b] Department of Civil Engineering, Colorado State University, Fort Collins, CO 80523, USA

Received 5 August 2003; received in revised form 5 August 2003

Abstract

Analytical solutions are derived for the cylindrical bending of multilayered, linear, and anisotropic magneto-electro-elastic plates under simple-supported edge conditions. We construct the general solution in terms of a simple formalism for any homogeneous layer, from which any physical quantities can be solved for the given boundary conditions. For multilayered plates, we derive the solution in terms of the propagator matrices. A special feature of cylindrical bending, which distinguishes itself from the three-dimensional plate problem, is that the associated eigenvalues for any homogeneous layer are independent of the sinusoidal mode, and thus need to be solved only once. Typical numerical examples are also presented for a piezomagnetic plate, a two-layered piezoelectric/piezomagnetic plate, and a four layered piezoelectric/piezomagnetic plate, with different span-to-thickness ratios. In particular, the piezoelectric and piezomagnetic fields show certain interesting features, which give guidance on the development of piezoelectric/piezomagnetic thin-plate theories. Furthermore, it is shown that the variations of the elastic, electric, and magnetic quantities with thickness depend strongly upon the material property and layering, which could be useful in the analysis and design of smart composite structures with sensors/actuators.

1. Introduction

Multilayered smart structures made of piezoelectric and piezomagnetic materials offer certain potential performance advantages over conventional composites, largely due to their unique capability of converting the system energy from one type to the other (among magnetic, electric, and mechanical energies) (Berlingcourt et al., 1964; Landau and Lifshitz, 1984; Harshe et al., 1993; Avellaneda and Harshe, 1994; Nan, 1994; Benveniste, 1995). While various numerical studies have been carried out to assist the design of composite laminates consisted of elastic and piezoelectric materials (Pagano, 1969, 1970; Tzou, 1993; Tzou and Tseng, 1990; Tzou and Ye, 1996; Bisegna and Maceri, 1996; Heyliger and Brooks, 1996; Lee and Jiang, 1996; Heyliger, 1997; Lee and Saravanos, 1997, 2000; Vel and Batra, 2000), investigation for the

* Corresponding author. Tel.: +1-330-972-6739; fax: +1-330-972-6020.
E-mail address: pan2@uakron.edu (E. Pan).

0020-7683/$ - see front matter © 2003 Elsevier Ltd. All rights reserved.
doi:10.1016/j.ijsolstr.2003.08.003

corresponding multilayered piezoelectric and piezomagnetic structures has only been started recently. Under the assumption of static deformation, Pan (2001) derived an exact closed-form solution for the multilayered piezoelectric and piezomagnetic plates based on the quasi-Stroh formalism and the propagator matrix method. It was observed that under a surface mechanical load, the piezoelectric (piezomagnetic) fields could be substantially enhanced in the piezoelectric (piezomagnetic) layer (Pan, 2001). More recently, Pan and Heyliger (2002) solved the corresponding vibration problem where they identified several modes that are purely elastic and independent of the piezoelectric/piezomagnetic coupling.

In this paper, we apply the analytical method to the static bending analysis of anisotropic, magneto-electro-elastic, and multilayered plates with simply supported edges. First, we derive the general solution for a homogeneous plate in terms of the Stroh-type formalism. A very distinguishing feature between the two-dimensional (2D) bending and three-dimensional (3D) deformation is that the eigenvalues for the homogeneous plate in the 2D bending need to be solved only once since they are independent of the eigenmode p (to be defined later). This is particularly useful when the solution is expressed in terms of the Fourier series and then summed together (Timoshenko and Woinowsky-Krieger, 1987; Bisegna and Maceri, 1996). To handle multilayered plates, the propagator matrix method (Gilbert and Backus, 1966; Pan, 1991, 1997) is again employed with which the corresponding multilayered solution has an elegant and simple expression.

Numerical examples are presented for different span-to-thickness ratios and for three representative plates: a single homogeneous magnetostrictive plate made of $CoFe_2O_4$, a two-layered plate of equal thickness with magnetostrictive $CoFe_2O_4$ in the top layer and piezoelectric $BaTiO_3$ in the bottom layer, and a four-layered plate Orth$-45/BaTiO_3/CoFe_2O_4$ /Orth$+45$ where Orth ± 45 are the orthotropic piezoelectric PZT-4 rotated ± 45 degrees with respect to the global x-axis. When approaching the thin-plate limit, we observed that while the behaviors of the elastic fields (elastic displacements and stresses) follow those in the purely elastic plate, the electric and magnetic fields showed certain different and new features that require particular consideration. Specifically, we find that the variation along the thickness-direction for the electric and magnetic potentials is usually of polynomial behavior with the order higher than that for the elastic displacements. Similarly, the electric displacement and magnetic flux fields are higher order polynomial functions of the thickness coordinates than those of the stresses. This implies that in the development of a thin-plate theory for the magneto-electro-elastic structure, a high order polynomial is needed for the electric and magnetic quantities. Finally, we have observed that different lay-ups result in totally different responses on the elastic, electric, and magnetic quantities. These general characteristics could be useful in the analysis and design of magneto-electro-elastic composite laminates.

2. Problem description and governing equations

We consider an anisotropic, magneto-electro-elastic, and N-layered rectangular plate with a finite horizontal dimension l in the y-direction. The plate is infinite in the x-direction and the thickness is in the (vertical) z-direction with a total thickness h. We assume that its two edges are simply supported as described by the end conditions on the laminate. A Cartesian coordinate system $(x, y, z) = (x_1, x_2, x_3)$ is attached to the plate in such a way that its origin is at the left-bottom corner and plate is in the positive z region. Layer j is bonded by the lower interface z_j and the upper interface z_{j+1} with thickness $h_j = z_{j+1} - z_j$. It is obvious that $z_1 = 0$ and $z_{N+1} = h$. Along the interface, the extended displacement and traction vectors (to be defined later) are assumed to be continuous. On the top and bottom surfaces of the layered plate, suitable boundary conditions can be described as will be discussed later on.

We start with a linear, anisotropic, and magneto-electro-elastic solid for which the coupled constitutive relation can be written as (Harshe et al., 1993; Nan, 1994; Benveniste, 1995; Pan, 2001)

$$\begin{aligned}\sigma_i &= C_{ik}\gamma_k - e_{ki}E_k - q_{ki}H_k\\ D_i &= e_{ik}\gamma_k + \varepsilon_{ik}E_k + d_{ik}H_k\\ B_i &= q_{ik}\gamma_k + d_{ik}E_k + \mu_{ik}H_k\end{aligned} \tag{1}$$

where σ_i, D_i, and B_i are the stress, electric displacement, and magnetic induction (i.e., magnetic flux), respectively; γ_i, E_i and H_i are the strain, electric field and magnetic field, respectively; C_{ij}, ε_{ij} and μ_{ij} are the elastic, dielectric, and magnetic permeability coefficients, respectively; e_{ij}, q_{ij}, and d_{ij} are the piezoelectric, piezomagnetic, and magnetoelectric coefficients, respectively. It is apparent that various uncoupled cases can be reduced from Eq. (1) by setting the appropriate coupling coefficients (e_{ij}, q_{ij}, and d_{ij}) to zero.

For a monoclinic material with poling direction coincident with the x_3 (or z) axis to be considered in this paper, the material constant matrices of Eq. (1) are expressed by

$$[C] = \begin{bmatrix} C_{11} & C_{12} & C_{13} & 0 & 0 & C_{16}\\ & C_{22} & C_{23} & 0 & 0 & C_{26}\\ & & C_{33} & 0 & 0 & C_{36}\\ & & & C_{44} & C_{45} & 0\\ & Sym & & & C_{55} & 0\\ & & & & & C_{66}\end{bmatrix}, \quad [e] = \begin{bmatrix} 0 & 0 & e_{31}\\ 0 & 0 & e_{32}\\ 0 & 0 & e_{33}\\ e_{14} & e_{24} & 0\\ e_{15} & e_{25} & 0\\ 0 & 0 & e_{36}\end{bmatrix}, \quad [q] = \begin{bmatrix} 0 & 0 & q_{31}\\ 0 & 0 & q_{32}\\ 0 & 0 & q_{33}\\ q_{14} & q_{24} & 0\\ q_{15} & q_{25} & 0\\ 0 & 0 & q_{36}\end{bmatrix} \tag{2}$$

$$[\varepsilon] = \begin{bmatrix} \varepsilon_{11} & \varepsilon_{12} & 0\\ \varepsilon_{12} & \varepsilon_{22} & 0\\ 0 & 0 & \varepsilon_{33}\end{bmatrix}, \quad [d] = \begin{bmatrix} d_{11} & d_{12} & 0\\ d_{12} & d_{22} & 0\\ 0 & 0 & d_{33}\end{bmatrix}, \quad [\mu] = \begin{bmatrix} \mu_{11} & \mu_{12} & 0\\ \mu_{12} & \mu_{22} & 0\\ 0 & 0 & \mu_{33}\end{bmatrix} \tag{3}$$

The general strain (using tensor symbol for the elastic strain γ_{ik})–displacement relation is

$$\begin{aligned}\gamma_{ij} &= 0.5(u_{i,j} + u_{j,i})\\ E_i &= -\phi_{,i}, \quad H_i = -\psi_{,i}\end{aligned} \tag{4}$$

where u_i, ϕ, and ψ are the elastic displacement, electric potential, and magnetic potential, respectively.

Assuming absence of the body force, electric charge, and current, the equilibrium equations are

$$\sigma_{ij,j} = 0; \quad D_{j,j} = 0; \quad B_{j,j} = 0 \tag{5}$$

3. General solutions

We seek the general two-dimensional solution of the *extended* displacement $\boldsymbol{u}(y,z)$ in the following form

$$\boldsymbol{u} \equiv \begin{bmatrix} u_1\\ u_2\\ u_3\\ \phi\\ \psi\end{bmatrix} = \mathrm{e}^{psz}\begin{bmatrix} a_1\cos py\\ a_2\cos py\\ a_3\sin py\\ a_4\sin py\\ a_5\sin py\end{bmatrix} \tag{6}$$

where s is the eigenvalue and a_i ($i = 1$–5) the corresponding eigenvector to be determined, and

$$p = n\pi/l \tag{7}$$

with n being a positive integer.

Substitution of Eq. (6) into the strain–displacement relation (4) and subsequently into the constitutive relation (1) yields the *extended* traction vector

$$\boldsymbol{t} \equiv \begin{bmatrix} \sigma_{13} \\ \sigma_{23} \\ \sigma_{33} \\ D_3 \\ B_3 \end{bmatrix} = p\mathrm{e}^{psz} \begin{bmatrix} b_1 \cos py \\ b_2 \cos py \\ b_3 \sin py \\ b_4 \sin py \\ b_5 \sin py \end{bmatrix} \tag{8}$$

Introducing two vectors

$$\boldsymbol{a} = [a_1, a_2, a_3, a_4, a_5]^{\mathrm{t}}, \quad \boldsymbol{b} = [b_1, b_2, b_3, b_4, b_5]^{\mathrm{t}} \tag{9}$$

we then find that vector $\boldsymbol{b}$ is related to $\boldsymbol{a}$ by the following relation

$$\boldsymbol{b} = (-\boldsymbol{R}^{\mathrm{t}} + s\boldsymbol{T})\boldsymbol{a} = -\frac{1}{s}(\boldsymbol{Q} + s\boldsymbol{R})\boldsymbol{a} \tag{10}$$

where the superscript 't' denotes matrix transpose, and

$$\boldsymbol{R} = \begin{bmatrix} 0 & 0 & C_{36} & e_{36} & q_{36} \\ 0 & 0 & C_{23} & e_{32} & q_{32} \\ -C_{45} & -C_{44} & 0 & 0 & 0 \\ -e_{25} & -e_{24} & 0 & 0 & 0 \\ -q_{25} & -q_{24} & 0 & 0 & 0 \end{bmatrix}, \quad \boldsymbol{T} = \begin{bmatrix} C_{55} & C_{45} & 0 & 0 & 0 \\ & C_{44} & 0 & 0 & 0 \\ & & C_{33} & e_{33} & q_{33} \\ & Sym & & -\varepsilon_{33} & -d_{33} \\ & & & & -\mu_{33} \end{bmatrix} \tag{11}$$

$$\boldsymbol{Q} = \begin{bmatrix} -C_{66} & -C_{26} & 0 & 0 & 0 \\ & -C_{22} & 0 & 0 & 0 \\ & & -C_{44} & -e_{24} & -q_{24} \\ & Sym & & \varepsilon_{22} & d_{22} \\ & & & & \mu_{22} \end{bmatrix} \tag{12}$$

The in-plane stresses and electric and magnetic displacements can be found using the strain–displacement relation (4), Eqs. (6) and (8), which are given below as

$$\begin{bmatrix} \sigma_{11} \\ \sigma_{12} \\ \sigma_{22} \\ D_1 \\ D_2 \\ B_1 \\ B_2 \end{bmatrix} = p\mathrm{e}^{psz} \begin{bmatrix} c_1 \sin py \\ c_2 \sin py \\ c_3 \sin py \\ c_4 \cos py \\ c_5 \cos py \\ c_6 \cos py \\ c_7 \cos py \end{bmatrix} \tag{13}$$

where

$$\begin{bmatrix} c_1 \\ c_2 \\ c_3 \\ c_4 \\ c_5 \\ c_6 \\ c_7 \end{bmatrix} = \begin{bmatrix} -C_{16} & -C_{12} & C_{13}s & e_{31}s & q_{31}s \\ -C_{66} & -C_{26} & C_{36}s & e_{36}s & q_{36}s \\ -C_{26} & -C_{22} & C_{23}s & e_{32}s & q_{32}s \\ e_{15}s & e_{14}s & e_{14} & -\varepsilon_{12} & -d_{12} \\ e_{25}s & e_{24}s & e_{24} & -\varepsilon_{22} & -d_{22} \\ q_{15}s & q_{14}s & q_{14} & -d_{12} & -\mu_{12} \\ q_{25}s & q_{24}s & q_{24} & -d_{22} & -\mu_{22} \end{bmatrix} \begin{bmatrix} a_1 \\ a_2 \\ a_3 \\ a_4 \\ a_5 \end{bmatrix} \tag{14}$$

Satisfaction of Eq. (5) yields the following eigenproblem for the eigenvalue s and the corresponding eigenvector $\boldsymbol{a}$,

$$[\boldsymbol{Q} + s(\boldsymbol{R} + \boldsymbol{R}') + s^2\boldsymbol{T}]\boldsymbol{a} = 0 \tag{15}$$

where $\boldsymbol{R}' = -\boldsymbol{R}^{\mathrm{t}}$.

It is noted that Eq. (15), derived for a simply supported plate, resembles the Stroh formalism (Stroh, 1958; Ting, 1996). However, their solution structures are different because of the slightly different features of the involved matrices (Pan, 2001).

To solve the eigenproblem (15), we can first recast it, with aid of Eq. (10), into a 10×10 linear eigensystem

$$\boldsymbol{N}\begin{bmatrix}\boldsymbol{a}\\ \boldsymbol{b}\end{bmatrix} = s\begin{bmatrix}\boldsymbol{a}\\ \boldsymbol{b}\end{bmatrix} \tag{16}$$

where

$$\boldsymbol{N} = \begin{bmatrix} -\boldsymbol{T}^{-1}\boldsymbol{R}' & \boldsymbol{T}^{-1} \\ -\boldsymbol{Q} + \boldsymbol{R}\boldsymbol{T}^{-1}\boldsymbol{R}' & -\boldsymbol{R}\boldsymbol{T}^{-1} \end{bmatrix} \tag{17}$$

It has been proved (Pan, 2001) that if s is an eigenvalue of Eq. (16), so is $-s$. Therefore, we can assume that the first five eigenvalues have positive real parts (if the real part is zero, then we pick the eigenvalue with positive imaginary part) and the last five have opposite signs to the first five. We distinguish the corresponding 10 eigenvectors by attaching a subscript to $\boldsymbol{a}$ and $\boldsymbol{b}$. Then the general solution for the extended displacement and traction vectors (of the z-dependent, y-independent factor) are derived as

$$\begin{bmatrix}\boldsymbol{u}\\ \boldsymbol{t}\end{bmatrix} = \begin{bmatrix}\boldsymbol{A}_1 & \boldsymbol{A}_2\\ \boldsymbol{B}_1 & \boldsymbol{B}_2\end{bmatrix}\langle \mathrm{e}^{ps^* z}\rangle \begin{bmatrix}\boldsymbol{K}_1\\ \boldsymbol{K}_2\end{bmatrix} \tag{18}$$

where

$$\begin{aligned} &\boldsymbol{A}_1 = [\boldsymbol{a}_1, \boldsymbol{a}_2, \boldsymbol{a}_3, \boldsymbol{a}_4, \boldsymbol{a}_5], \quad \boldsymbol{A}_2 = [\boldsymbol{a}_6, \boldsymbol{a}_7, \boldsymbol{a}_8, \boldsymbol{a}_9, \boldsymbol{a}_{10}]\\ &\boldsymbol{B}_1 = [\boldsymbol{b}_1, \boldsymbol{b}_2, \boldsymbol{b}_3, \boldsymbol{b}_4, \boldsymbol{b}_5], \quad \boldsymbol{B}_2 = [\boldsymbol{b}_6, \boldsymbol{b}_7, \boldsymbol{b}_8, \boldsymbol{b}_9, \boldsymbol{b}_{10}]\\ &\langle \mathrm{e}^{ps^* z}\rangle = \mathrm{diag}[\mathrm{e}^{ps_1 z}, \mathrm{e}^{ps_2 z}, \mathrm{e}^{ps_3 z}, \mathrm{e}^{ps_4 z}, \mathrm{e}^{ps_5 z}, \mathrm{e}^{-ps_1 z}, \mathrm{e}^{-ps_2 z}, \mathrm{e}^{-ps_3 z}, \mathrm{e}^{-ps_4 z}, \mathrm{e}^{-ps_5 z}] \end{aligned} \tag{19}$$

and $\boldsymbol{K}_1$ and $\boldsymbol{K}_2$ are 5×1 column matrices to be determined.

We note a distinct difference between the cylindrical deformation here and the rectangular plate deformation studied in Pan (2001): While the ten roots in the rectangular plate case depend on the deformation modes (p, q), for the cylindrical case, they are independent of the model parameter p defined in (7). In other words, the roots in the cylindrical case depend only on the material properties. This is particularly advantageous when solving a general boundary value problem where the given loading will be expressed in terms of the Fourier series, and the solution is the sum of each Fourier term.

With Eq. (18) being served as a general solution for a homogeneous and magneto-electro-elastic plate, the solution for the corresponding layered plate can be derived using the continuity conditions along the interface and the boundary conditions on the top and bottom surfaces of the plate. In so doing, a system of linear equations for the unknowns can be formed and solved (Heyliger and Brooks, 1996; Heyliger, 1997). For structures with relatively large numbers of layers (up to a hundred layers), however, the system of linear equations becomes very large, and the propagator matrix method developed exclusively for layered structures can be conveniently and efficiently applied (for a brief review, see Pan, 1997). We discuss this approach in the next section.

4. Propagator matrix for a layered system

Since the matrix $\boldsymbol{N}$, defined in Eq. (17), is not symmetric, the eigenvectors of Eq. (16) are actually the right ones. The left eigenvectors are found by solving the following eigenvalue system

$$\boldsymbol{N}^{\mathrm{t}}\boldsymbol{\eta} = \lambda\boldsymbol{\eta} \tag{20}$$

It is known that if s and $[\boldsymbol{a}, \boldsymbol{b}]^{\mathrm{t}}$ are the eigenvalue and eigenvector solutions of Eq. (16), then $\lambda = -s$ and $\boldsymbol{\eta} = [-\boldsymbol{b}, \boldsymbol{a}]^{\mathrm{t}}$ are the corresponding solutions of Eq. (20). The orthogonality of the left and right eigenvectors yields the following important relation:

$$\begin{bmatrix} -\boldsymbol{B}_2^{\mathrm{t}} & \boldsymbol{A}_2^{\mathrm{t}} \\ \boldsymbol{B}_1^{\mathrm{t}} & -\boldsymbol{A}_1^{\mathrm{t}} \end{bmatrix} \begin{bmatrix} \boldsymbol{A}_1 & \boldsymbol{A}_2 \\ \boldsymbol{B}_1 & \boldsymbol{B}_2 \end{bmatrix} = \begin{bmatrix} \boldsymbol{I} & \boldsymbol{0} \\ \boldsymbol{0} & \boldsymbol{I} \end{bmatrix} \tag{21}$$

where $\boldsymbol{I}$ is a 5×5 identical matrix, and the eigenvectors have been normalized according to

$$-\boldsymbol{B}_2^{\mathrm{t}}\boldsymbol{A}_1 + \boldsymbol{A}_2^{\mathrm{t}}\boldsymbol{B}_1 = \boldsymbol{I} \tag{22}$$

Eq. (21) resembles the orthogonal relation in the Stroh formalism (Ting, 1996) and provides us a simple way of inverting the eigenvector matrix, which is required in forming the propagator matrix.

Let us assume that Eq. (18) is a general solution in the homogeneous layer j, with top and bottom boundaries at z and 0 (locally). Letting $z = 0$ in Eq. (18) and solving for the unknown column matrices, we find

$$\begin{bmatrix} \boldsymbol{K}_1 \\ \boldsymbol{K}_2 \end{bmatrix} = \begin{bmatrix} \boldsymbol{A}_1 & \boldsymbol{A}_2 \\ \boldsymbol{B}_1 & \boldsymbol{B}_2 \end{bmatrix}^{-1} \begin{bmatrix} \boldsymbol{u} \\ \boldsymbol{t} \end{bmatrix}_0 = \begin{bmatrix} -\boldsymbol{B}_2^{\mathrm{t}} & \boldsymbol{A}_2^{\mathrm{t}} \\ \boldsymbol{B}_1^{\mathrm{t}} & -\boldsymbol{A}_1^{\mathrm{t}} \end{bmatrix} \begin{bmatrix} \boldsymbol{u} \\ \boldsymbol{t} \end{bmatrix}_0 \tag{23}$$

The second equation follows from Eq. (21). Therefore, the solution in the homogeneous layer j at any z can be expressed by that at $z = 0$, i.e.,

$$\begin{bmatrix} \boldsymbol{u} \\ \boldsymbol{t} \end{bmatrix}_z = \boldsymbol{P}(z) \begin{bmatrix} \boldsymbol{u} \\ \boldsymbol{t} \end{bmatrix}_0 \tag{24}$$

where

$$\boldsymbol{P}(z) = \begin{bmatrix} \boldsymbol{A}_1 & \boldsymbol{A}_2 \\ \boldsymbol{B}_1 & \boldsymbol{B}_2 \end{bmatrix} \langle \mathrm{e}^{ps*z} \rangle \begin{bmatrix} -\boldsymbol{B}_2^{\mathrm{t}} & \boldsymbol{A}_2^{\mathrm{t}} \\ \boldsymbol{B}_1^{\mathrm{t}} & -\boldsymbol{A}_1^{\mathrm{t}} \end{bmatrix} \tag{25}$$

is called the propagator matrix (Gilbert and Backus, 1966; Pan, 1997).

The propagating relation (24) can be used repeatedly so that we can propagate the physical quantities from the bottom surface $z = 0$ to the top surface $z = h$ of the layered plate. Consequently, we have

$$\begin{bmatrix} \boldsymbol{u} \\ \boldsymbol{t} \end{bmatrix}_H = \boldsymbol{P}_N(h_N)\boldsymbol{P}_{N-1}(h_{N-1}) \cdots \boldsymbol{P}_2(h_2)\boldsymbol{P}_1(h_1) \begin{bmatrix} \boldsymbol{u} \\ \boldsymbol{t} \end{bmatrix}_0 \tag{26}$$

where $h_j = z_{j+1} - z_j$ is the thickness of layer j and $\boldsymbol{P}_j$ the propagator matrix of layer j.

Table 1
Material coefficients of the magnetostrictive $CoFe_2O_4$ (C_{ij} in 10^9 N/m^2, q_{ij} in N/(A m), ε_{ij} in 10^{-9} C^2/(N m^2), and μ_{ij} in 10^{-6} N s^2/C^2)

$C_{11} = C_{22}$	C_{12}	$C_{13} = C_{23}$	C_{33}	$C_{44} = C_{55}$	$C_{66} = 0.5(C_{11} - C_{12})$
286	173	170.5	269.5	45.3	56.5
$q_{31} = q_{32}$	q_{33}	$q_{24} = q_{15}$			
580.3	699.7	550			
$\varepsilon_{11} = \varepsilon_{22}$	ε_{33}		$\mu_{11} = \mu_{22}$	μ_{33}	
0.08	0.093		−590	157	

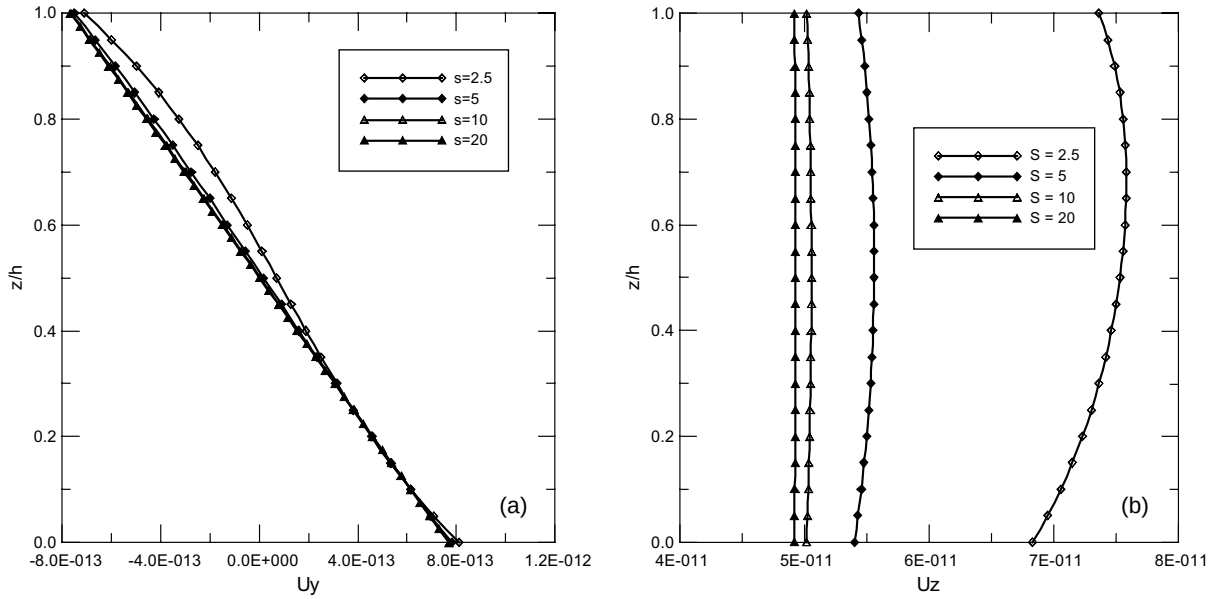

Fig. 1. (a) Variation of elastic displacement component u_y (in m) along the thickness direction of the single magnetostrictive $CoFe_2O_4$ plate for four different span-to-thickness ratios S. (b) Variation of elastic displacement component u_z (in m) along the thickness direction of the single magnetostrictive $CoFe_2O_4$ plate for four different span-to-thickness ratios S.

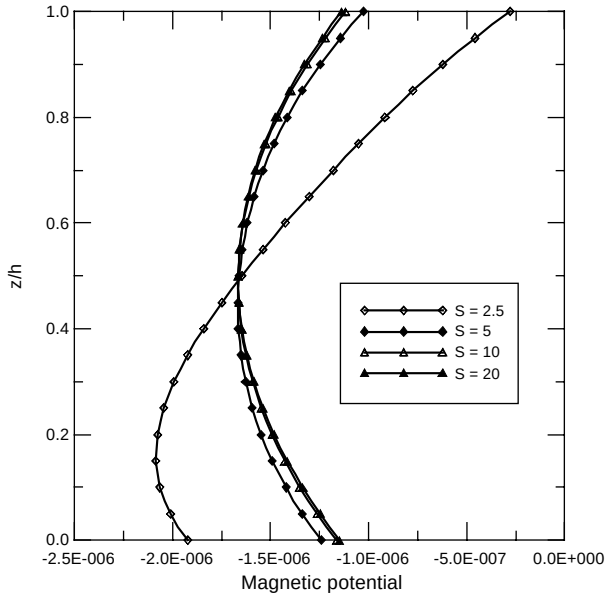

Fig. 2. Variation of magnetic potential ψ (in C/s) along the thickness direction of the single magnetostrictive $CoFe_2O_4$ plate for four different span-to-thickness ratios S.

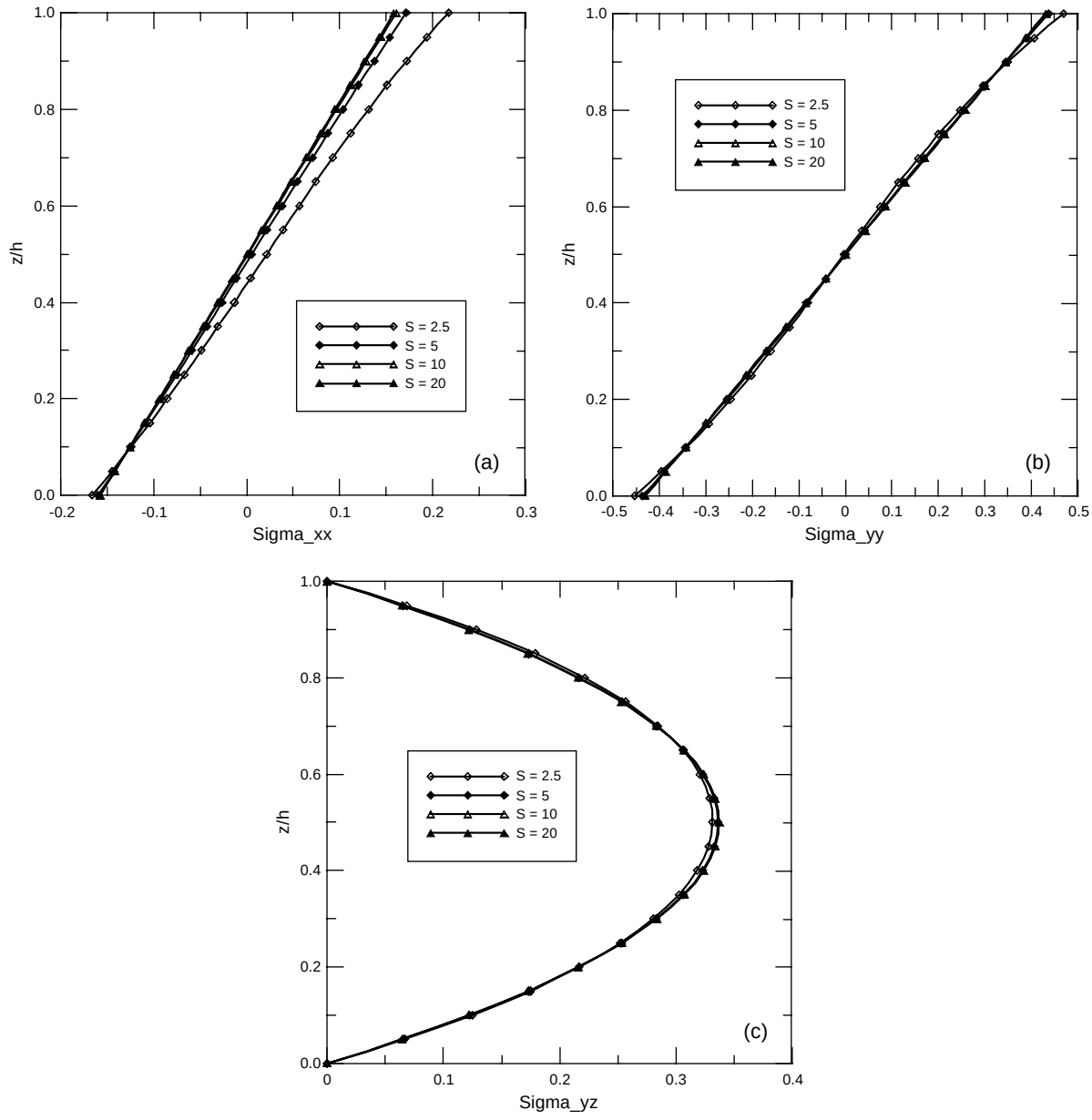

Fig. 3. (a) Variation of stress component σ_{xx} (in N/m^2) along the thickness direction of the single magnetostrictive $CoFe_2O_4$ plate for four different span-to-thickness ratios S. (b) Variation of stress component σ_{yy} (in N/m^2) along the thickness direction of the single magnetostrictive $CoFe_2O_4$ plate for four different span-to-thickness ratios S. (c) Variation of stress component σ_{yz} (in N/m^2) along the thickness direction of the single magnetostrictive $CoFe_2O_4$ plate for four different span-to-thickness ratios S.

Eq. (26) is a surprisingly simple relation and, for given boundary conditions, can be solved for the unknowns involved. In the following examples, we assume that the bottom surface ($z = 0$) is traction free

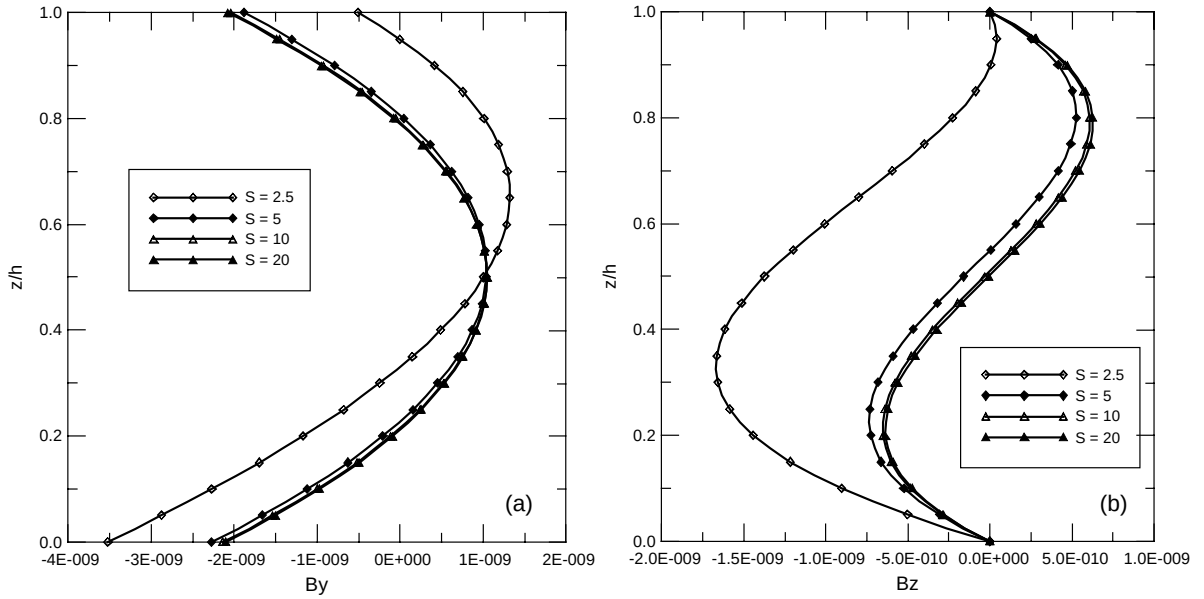

Fig. 4. (a) Variation of magnetic flux component B_y (in Wb/m^2) along the thickness direction of the single magnetostrictive $CoFe_2O_4$ plate for four different span-to-thickness ratios S. (b) Variation of magnetic flux component B_z (in Wb/m^2) along the thickness direction of the single magnetostrictive $CoFe_2O_4$ plate for four different span-to-thickness ratios S.

Table 2
Material coefficients of the piezoelectric $BaTiO_3$ (C_{ij} in 10^9 N/m^2, e_{ij} in C/m^2, ε_{ij} in 10^{-9} C^2/(N m^2), and μ_{ij} in 10^{-6} N s^2/C^2)

$C_{11} = C_{22}$	C_{12}	$C_{13} = C_{23}$	C_{33}	$C_{44} = C_{55}$	$C_{66} = 0.5(C_{11} - C_{12})$
166	77	78	162	43	44.5
$e_{31} = e_{32}$	e_{33}	$e_{24} = e_{15}$			
−4.4	18.6	11.6			
$\varepsilon_{11} = \varepsilon_{22}$	ε_{33}		$\mu_{11} = \mu_{22}$	μ_{33}	
11.2	12.6		5	10	

(i.e., the elastic traction and the z-direction electric displacement and magnetic induction are zero) and that on the top surface ($z = h$), we give

$$\boldsymbol{t}(H) = [0, 0, \sigma_0 \sin py, 0, 0]^{\mathrm{t}} \tag{27}$$

5. Numerical examples

In the examples presented below, the span-to-thickness ratios $S \equiv l/h$ ($h = 1m$) are equal to 2.5, 5, 10, and 20. A sinusoidal load is applied at the top surface $z = h$ (in meter), as given by Eq. (27) with $\sigma_0 = 1$ N/m^2 Furthermore, n in Eq. (7) is fixed at 1 and y is at $S/4$. To study the thin-plate limit, we follow Pagano (1969, 1970) to normalize u_x and u_y by dividing S^3, u_z by multiplying $100/S^4$, σ_{xx}, σ_{yy}, and σ_{xy} by dividing S^2, and σ_{yz} and σ_{xz} by dividing S. Furthermore, the piezoelectric and piezomagnetic fields are also normalized, with ϕ and ψ being divided by S^2, D_x, D_y, B_x, and B_y divided by S. It is noted that in so doing all the physical quantities are still dimensional with the elastic displacement in m, stress in N/m^2, electric potential in V,

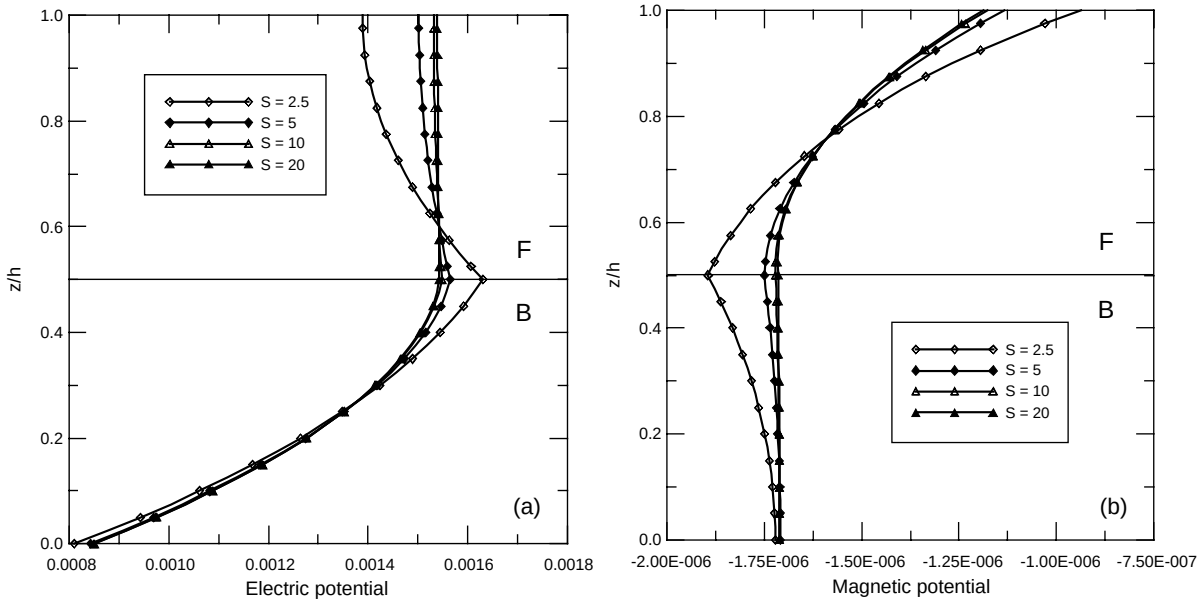

Fig. 5. (a) Variation of electric potential ϕ (in V) along the thickness direction of the two-layered F/B plate for four different span-to-thickness ratios S. (b) Variation of magnetic potential ψ (in C/s) along the thickness direction of the two-layered F/B plate for four different span-to-thickness ratios S.

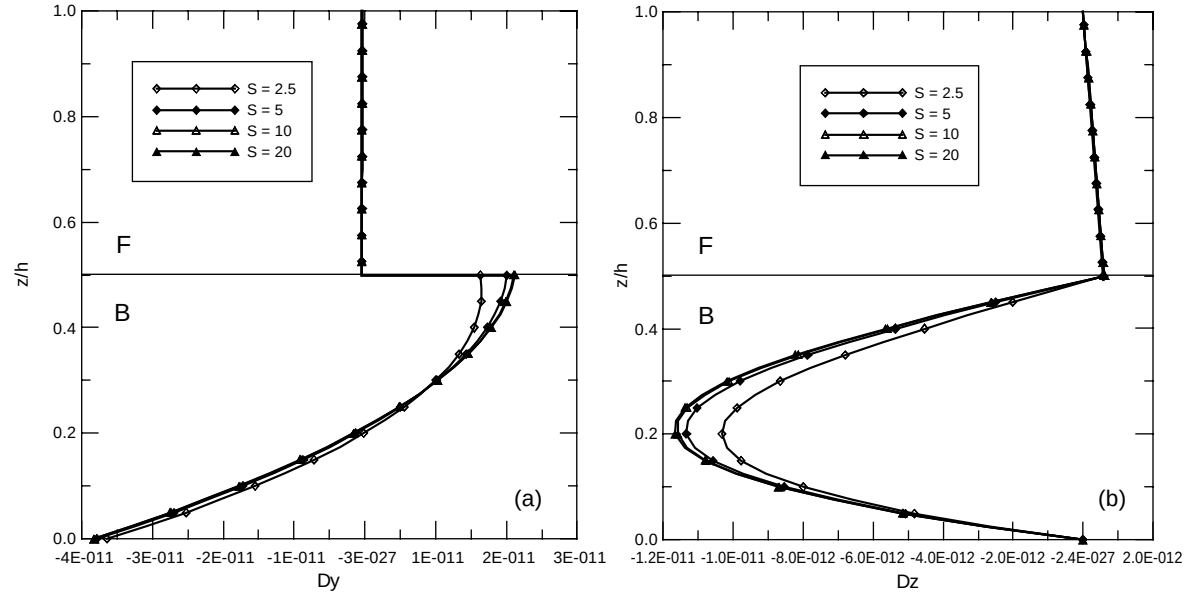

Fig. 6. (a) Variation of electric displacement component D_y (in C/m^2) along the thickness direction of the two-layered F/B plate for four different span-to-thickness ratios S. (b) Variation of electric displacement component D_z (in C/m^2) along the thickness direction of the two-layered F/B plate for four different span-to-thickness ratios S.

magnetic potential in C/s, electric displacement in C/m^2 and magnetic flux (or induction) in Wb/m^2. We also remark that results from our analytical model have been compared with those from a continuum-based discrete-layer plate theory with excellent agreement being obtained (Heyliger et al., 2002).

Example 1. The first example is a single layer model, which is made of the magnetostrictive $CoFe_2O_4$. The material properties of the layer are given in Table 1 (Pan, 2001).

The variation of the displacement components u_y and u_z along the thickness direction for different span-to-thickness ratios S are shown in Fig. 1a and b. As can be clearly observed, while u_y is a linear function of z in the thin-plate limit ($S = 20$), u_z is constant, demonstrating the general features for the purely elastic thin-plate theory. However, the magnetic potential is a quadratic function of z, as shown in Fig. 2.

The stress components are plotted in Fig. 3a–c, which show, in the thin-plate limit, a linear variation along the z-direction for the normal stress components σ_{xx} and σ_{yy} (Fig. 3a and b), and a quadratic variation for σ_{yz} (Fig. 3c). Again, these thin-plate stress distribution features are the same for the purely elastic case.

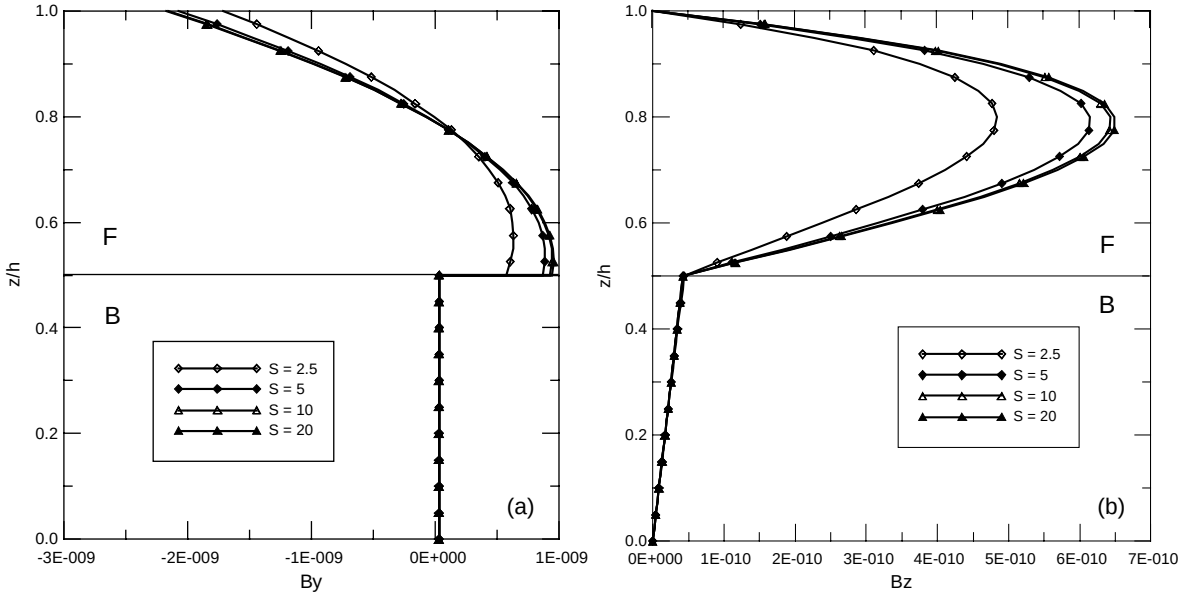

Fig. 7. (a) Variation of magnetic flux component B_y (in Wb/m^2) along the thickness direction of the two-layered F/B plate for four different span-to-thickness ratios S. (b) Variation of magnetic flux component B_z (in Wb/m^2) along the thickness direction of the two-layered F/B plate for four different span-to-thickness ratios S.

Table 3
Material coefficients of the orthotropic piezoelectric PZT-4 (C_{ij} in 10^9 N/m^2, e_{ij} in C/m^2, ε_{ij} in 10^{-9} C^2/(N m^2))

C_{11}	C_{22}	C_{33}	C_{44}	C_{55}	C_{66}
238	23.6	10.6	2.15	4.4	6.43
C_{12}	C_{13}	C_{23}		ε_{11}	$\varepsilon_{11} = \varepsilon_{22}$
3.98	2.19	1.92		0.110625	0.106023
	e_{31}	e_{32}	e_{33}	$e_{24} = e_{15}$	
	−0.13	−0.14	−0.28	−0.01	

The distributions of the magnetic flux components, however, are different. While B_y is quadratic in z (Fig. 4a), B_z is cubic in z (Fig. 4b). Therefore, in the thin-plate theory for the magneto-electro-elastic laminate, the magnetic and electric quantities would generally require a high-order polynomial approximation.

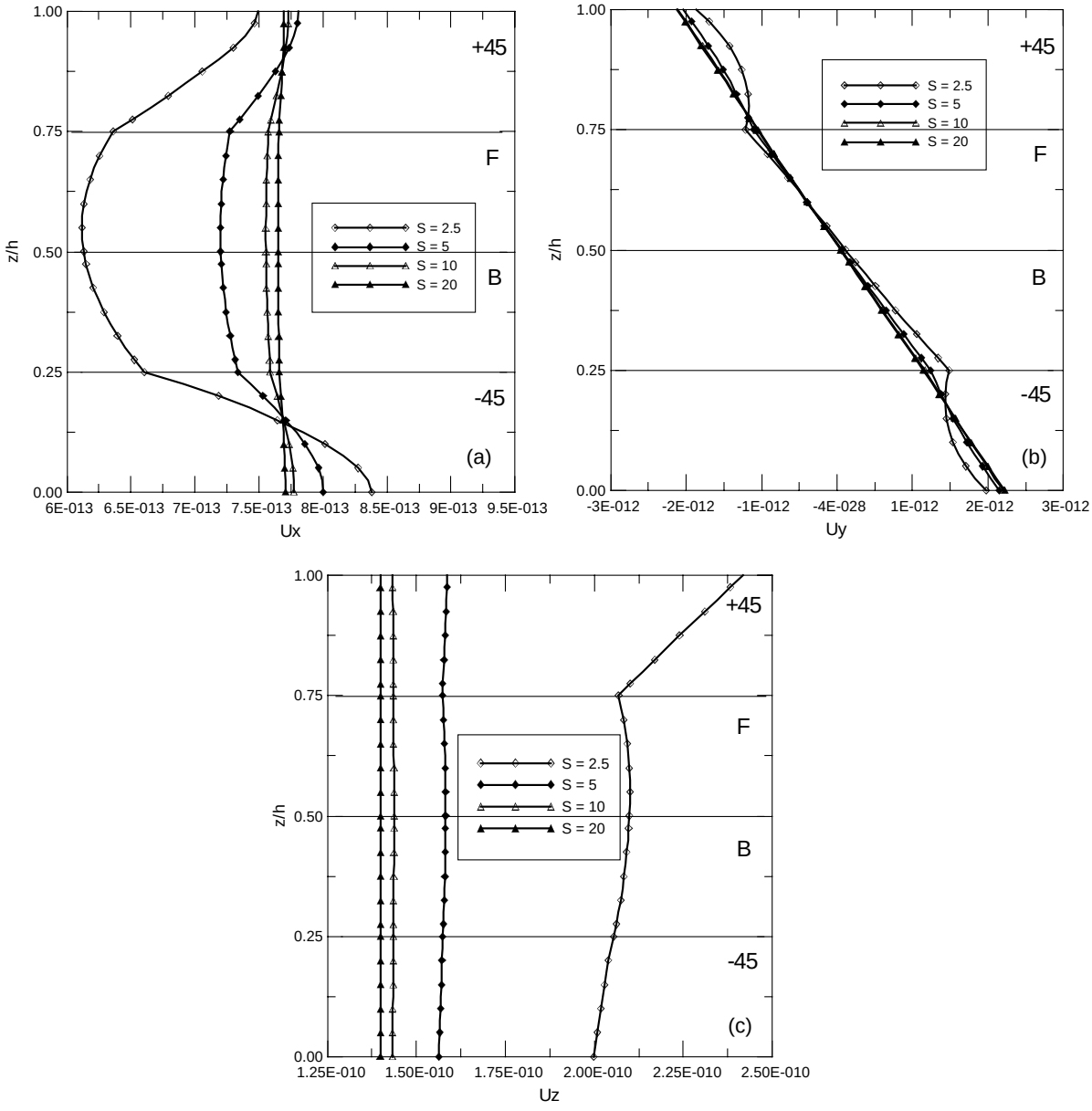

Fig. 8. (a) Variation of elastic component u_x (in m) along the thickness direction of the four-layered +45/F/B/−45 plate for four different span-to-thickness ratios S. (b) Variation of elastic component u_y (in m) along the thickness direction of the four-layered +45/F/B/−45 plate for four different span-to-thickness ratios S. (c) Variation of elastic component u_z (in m) along the thickness direction of the four-layered +45/F/B/−45 plate for four different span-to-thickness ratios S.

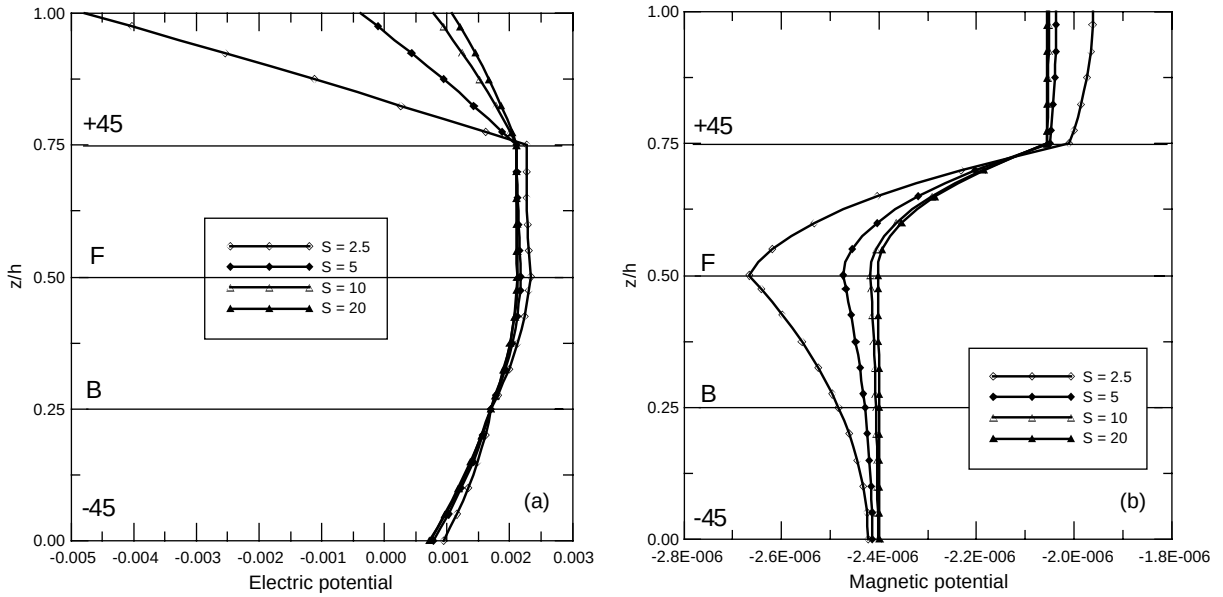

Fig. 9. (a) Variation of electric potential ϕ (in V) along the thickness direction of the four-layered +45/F/B/−45 plate for four different span-to-thickness ratios S. (b) Variation of magnetic potential ψ (in C/s) along the thickness direction of the four-layered +45/F/B/−45 plate for four different span-to-thickness ratios S.

Example 2. The second example is a two-layered plate made of piezoelectric $BaTiO_3$ with material properties given in Table 2 (Pan, 2001) and magnetostrictive $CoFe_2O_4$. The piezoelectric $BaTiO_3$ is in the bottom layer $(0 < z < 0.5h)$ and the magnetostrictive $CoFe_2O_4$ is in the top layer $(0.5h < z < h)$. Starting from the top, this two-layered plate is named as F/B plate.

Shown in Fig. 5a and b are, respectively, the variations of the electric and magnetic potentials along the z-direction for different span-to-thickness ratios S. It is interesting that, in the thin-plate limit, the electric (magnetic) potential in the thickness direction is nearly constant in the magnetostrictive (electric) layer, and is quadratic in the electric (magnetostrictive) layer. Similarly, the electric displacement components are either constant or linear in the magnetostrictive layer but are quadratic in the electric layer (Fig. 6a and b). An opposite behavior is observed for the magnetic flux components as shown in Fig. 7a and b, where they are quadratic functions of z in the magnetostrictive layer but constant or linear functions of z in the electric layer. We finally remark that the variation of the displacement components u_y and u_z along the thickness direction for different span-to-thickness ratios S is similar to the single plate case as shown in Fig. 1a and b.

Example 3. In the third example, the plate is made of four layers of equal thickness with each having a thickness of $0.25h$. The stacking sequence from the top to bottom is Orth+45/$CoFe_2O_4$/$BaTiO_3$/Orth−45, or +45/F/B/−45 for simplicity. While $BaTiO_3$ and $CoFe_2O_4$ are the materials used in Examples 1 and 2, materials Orth±45 are from PZT-4 by rotating ±45 degrees with respect to the x-axis. The properties of the orthotropic piezoelectric PZT-4 (Heyliger, 1997) are given in Table 3.

Fig. 8a–c show the variations of the elastic displacements along the z-direction for different span-to-thickness ratios S. As can be observed, they are either constant or linear functions of the thickness coordinate z.

While Fig. 9a shows the variation of the electric potential along the thickness direction, Fig. 9b plots that for the magnetic potential. A special feature is noticed for the variation of the electric potential in the top Orth+45 layer where it experiences a very large gradient from the top surface to the interface (Fig. 9a).

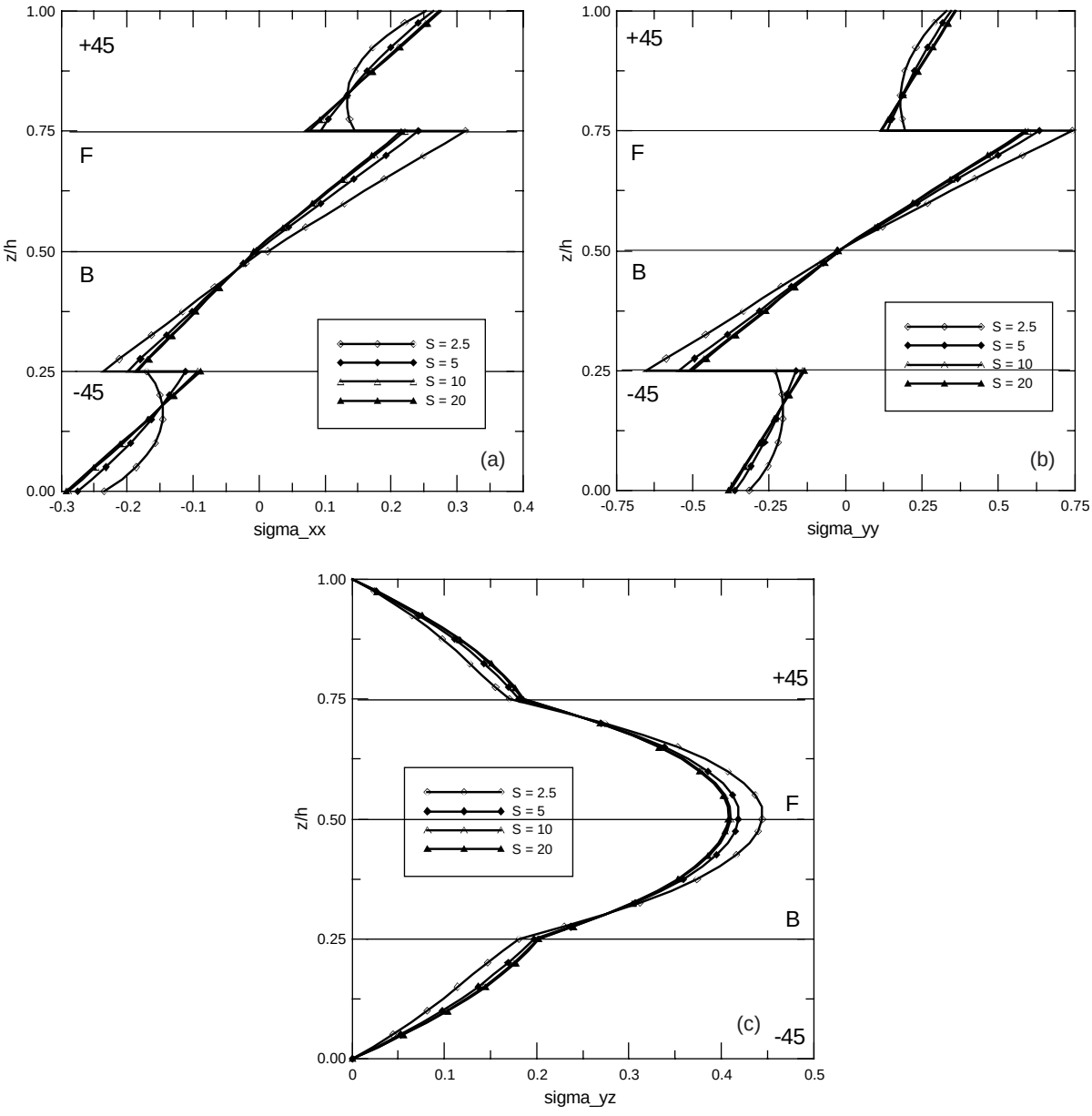

Fig. 10. (a) Variation of stress component σ_{xx} (in N/m^2) along the thickness direction of the four-layered +45/F/B/−45 plate for four different span-to-thickness ratios S. (b) Variation of stress component σ_{yy} (in N/m^2) along the thickness direction of the four-layered +45/F/B/−45 plate for four different span-to-thickness ratios S. (c) Variation of stress component σ_{yz} (in N/m^2) along the thickness direction of the four-layered +45/F/B/−45 plate for four different span-to-thickness ratios S. (d) Variation of stress component σ_{xz} (in N/m^2) along the thickness direction of the four-layered +45/F/B/−45 plate for four different span-to-thickness ratios S. (e) Variation of stress component σ_{xy} (in N/m^2) along the thickness direction of the four-layered +45/F/B/−45 plate for four different span-to-thickness ratios S.

The variations of the stress components along the thickness direction are shown in Fig. 10a–e. It is clearly observed, they are either a linear function of z (Fig. 10a, b, d, and e for σ_{xx}, σ_{yy}, σ_{xz} and σ_{xy}) or a

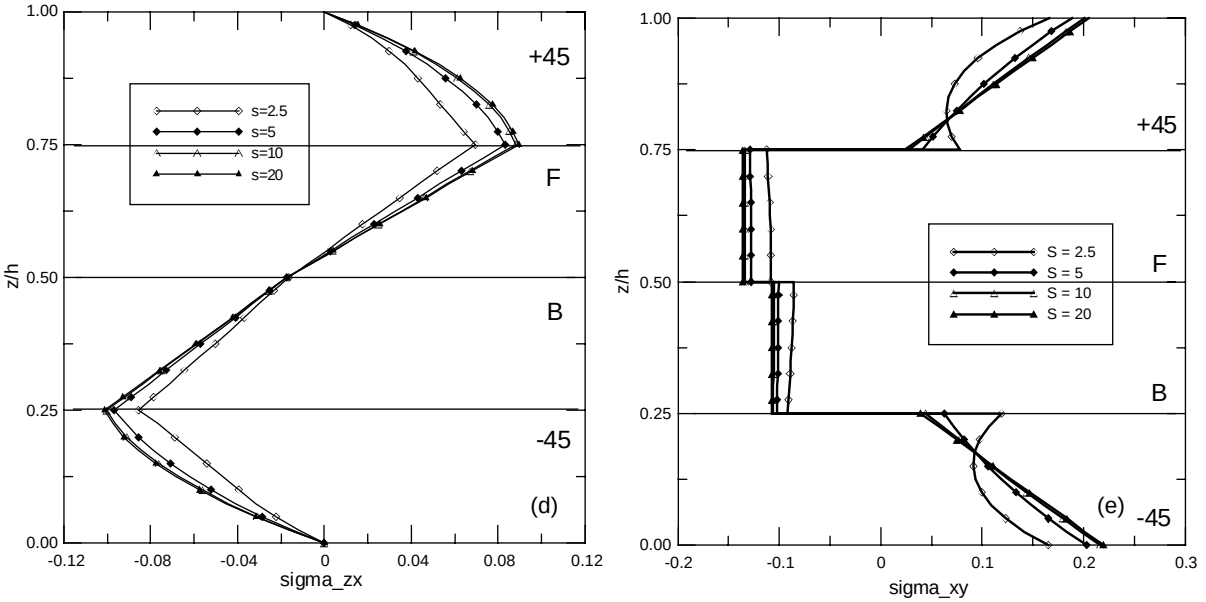

Fig. 10 (*continued*)

quadratic function of z (Fig. 10c for σ_{yz}). Again, these features are consistent with those observed from the purely elastic composite plates.

Finally, Fig. 11a–c and Fig. 12a–c show the variations of the electric displacement and magnetic flux. As can be seen, their variations are similar to those in the two-layered plate presented in Example 2. That is, the electric displacement has higher order variation in the electric layer than that in the magnetic layer (Fig. 11a–c). On the other hand, the magnetic flux has higher order variation in the magnetostrictive layer than that in the electric layer (Fig. 12a–c).

6. Conclusions

In this paper, we have derived an analytical solution for the static bending of an anisotropic, magneto-electro-elastic, and multilayered plate with simply supported edges. Similar to the analysis for the corresponding 3D plate problem, the homogeneous solutions are expressed in terms of the simple quasi-Stroh formalism and the solution in the multilayered plate in terms of the propagator matrix method. It is noted, however, while for the 3D plate case, the eigenvalues of the homogeneous plate depend on the eigenmode pair (p, q), for the 2D cylindrical bending, the eigenvalues are independent of the eigenmode p. Thus the homogeneous solution for each layer needs to be solved only once, independently of the eigenmode p. This is particularly efficient when superposing all the sinusoidal responses together as in the Fourier series summation.

Numerical examples are presented for three representative plates: a single homogeneous magnetostrictive plate made of $CoFe_2O_4$, a two-layered plate made of magnetostrictive $CoFe_2O_4$ in the top layer and piezoelectric $BaTiO_3$ in the bottom layer, and a four-layered plate Orth+45/$CoFe_2O_4$/$BaTiO_3$/Orth−45. For different span-to-thickness ratios, we have observed that, in the thin-plate limit, while the elastic fields (elastic displacements and stresses) follow those in the purely elastic plate, the electric and magnetic fields

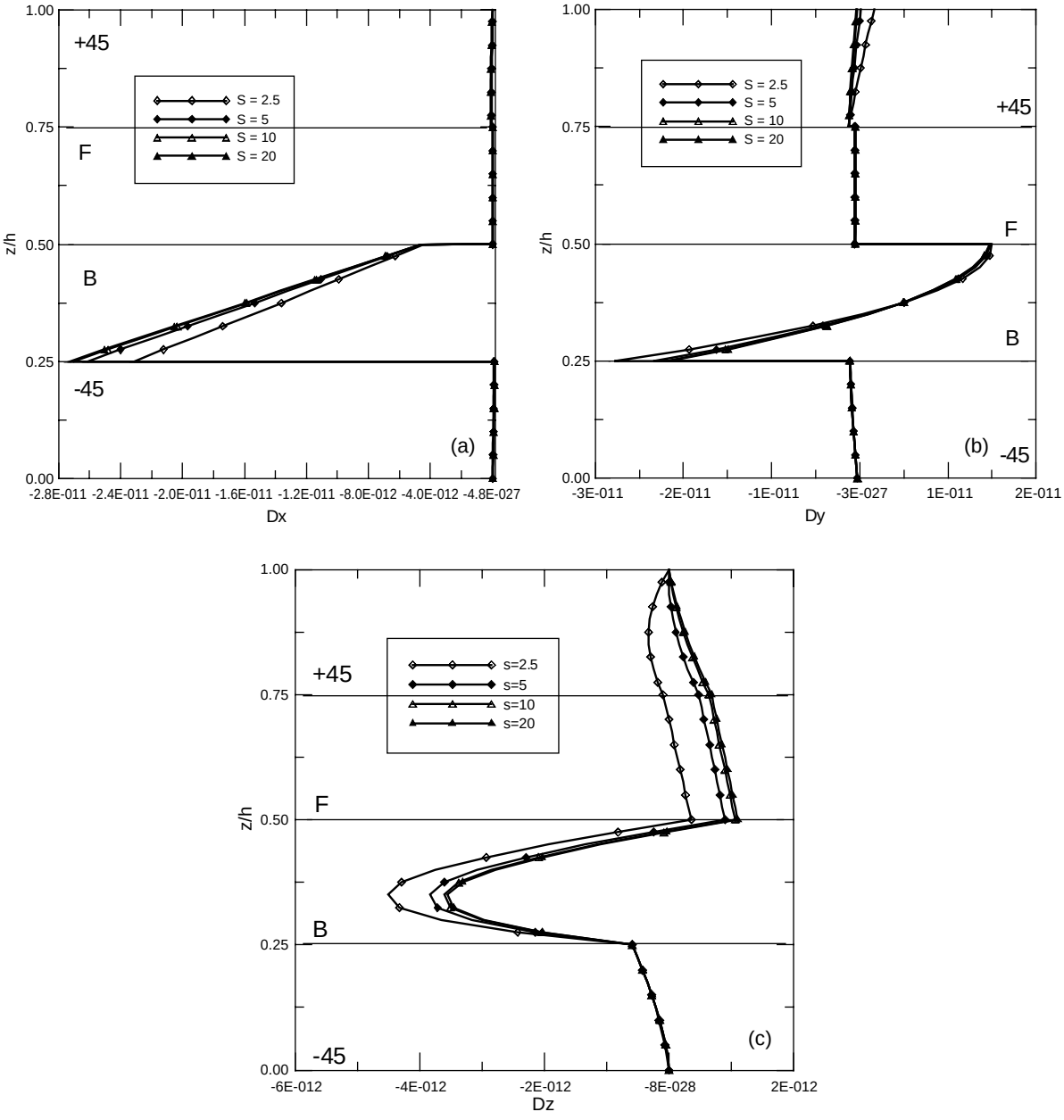

Fig. 11. (a) Variation of electric displacement component D_x (in C/m^2) along the thickness direction of the four-layered +45/F/B/−45 plate for four different span-to-thickness ratios S. (b) Variation of electric displacement component D_y (in C/m^2) along the thickness direction of the four-layered +45/F/B/−45 plate for four different span-to-thickness ratios S. (c) Variation of electric displacement component D_z (in C/m^2) along the thickness direction of the four-layered +45/F/B/−45 plate for four different span-to-thickness ratios S.

showed very different features. In particular, their variations along the thickness direction are usually high-order polynomial functions of the thickness coordinate. In other words, in the development of a thin-plate

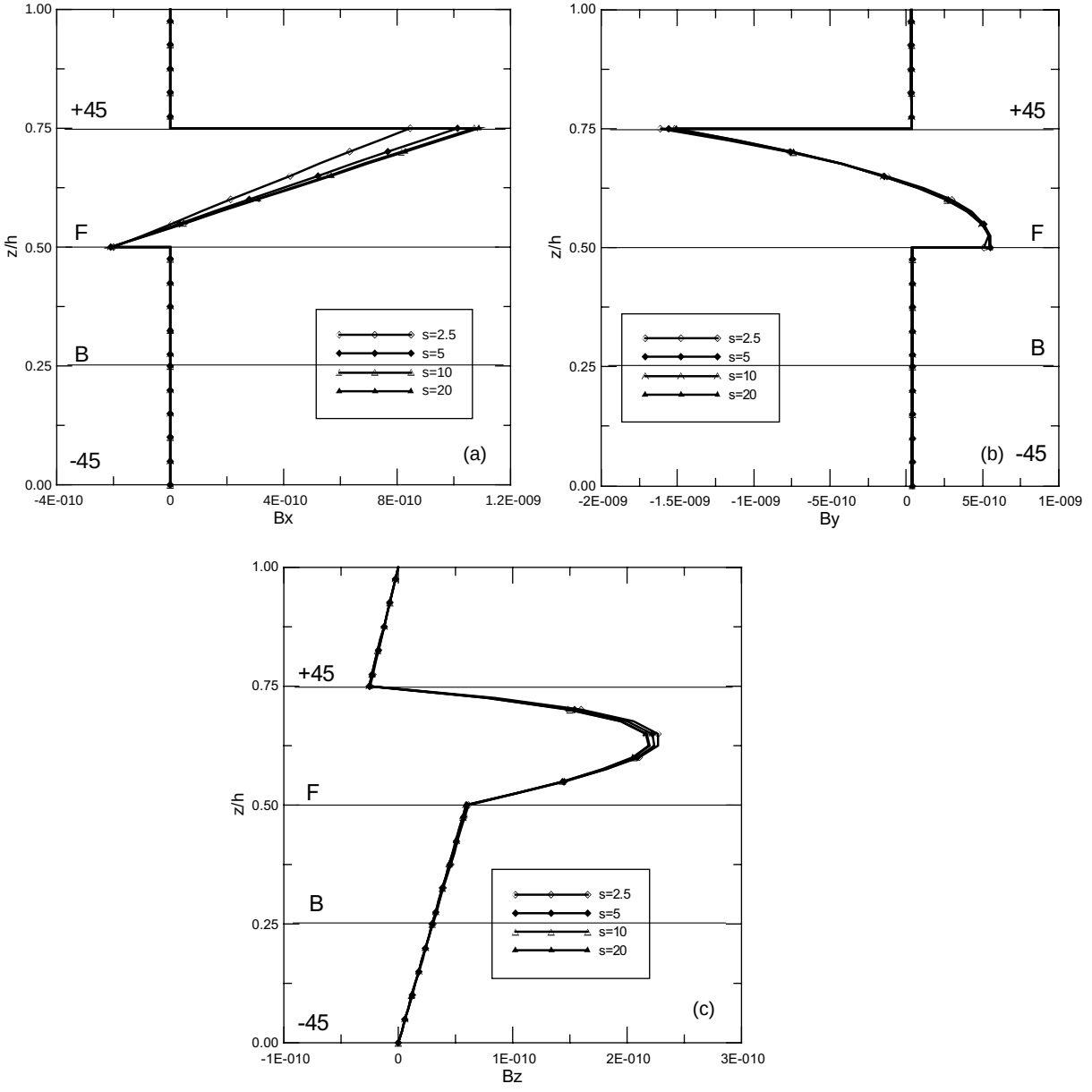

Fig. 12. (a) Variation of magnetic flux component B_x (in Wb/m^2) along the thickness direction of the four-layered +45/F/B/−45 plate for four different span-to-thickness ratios S. (b) Variation of magnetic flux component B_y (in Wb/m^2) along the thickness direction of the four-layered +45/F/B/−45 plate for four different span-to-thickness ratios S. (c) Variation of magnetic flux component B_z (in Wb/m^2) along the thickness direction of the four-layered +45/F/B/−45 plate for four different span-to-thickness ratios S.

theory for the magneto-electro-elastic plate, a high-order polynomial is needed for the electric and magnetic quantities. Finally, we have observed that different lay-ups could predict totally different responses on the elastic, electric, and magnetic quantities. These general features should be useful in the analysis and design of magneto-electro-elastic composite laminates.

References

Avellaneda, M., Harshe, G., 1994. Magnetoelectric effect in piezoelectric/magnetostrictive multiplayer (2–2) composites. J. Intelligent Mater. Syst. Struct. 5, 501–513.

Benveniste, Y., 1995. Magnetoelectric effect in fibrous composites with piezoelectric and piezomagnetic phases. Phys. Rev. B 51, 16424–16427.

Berlingcourt, D.A., Curran, D.R., Jaffe, H., 1964. Piezoelectric and piezomagnetic materials and their function in transducers. In: Physical Acoustics, vol. 1, pp. 169–270.

Bisegna, P., Maceri, F., 1996. An exact three-dimensional solution for simply supported rectangular piezoelectric plates. J. Appl. Mech. 63, 628–638.

Gilbert, F., Backus, G., 1966. Propagator matrices in elastic wave and vibration problems. Geophysics 31, 326–332.

Harshe, G., Dougherty, J.P., Newnham, R.E., 1993. Theoretical modeling of multiplayer magnetoelectric composites. Int. J. Appl. Eletromag. Mater. 4, 145–159.

Heyliger, P., 1997. Exact solutions for simply supported laminated piezoelectric plates. J. Appl. Mech. 64, 299–306.

Heyliger, P., Brooks, S., 1996. Exact solutions for laminated piezoelectric plates in cylindrical bending. J. Appl. Mech. 63, 903–910.

Heyliger, P.R., Ramirez, F., Pan, E., 2002. Static and dynamic response of laminated magnetoelectroelastic beams and plates. In: Proceedings of the 13th International Conference on Adaptive Structures and Technologies Potsdam, Germany, October 7–9, 2002.

Landau, L.D., Lifshitz, E.M., 1984. In: Lifshitz, E.M., Pitaevskii, L.P. (Eds.), Electrodynamics of Continuous Media, second edition. Pergamon Press, New York.

Lee, J.S., Jiang, L.Z., 1996. Exact electroelastic analysis of piezoelectric laminae via state space approach. Int. J. Solids Struct. 33, 977–990.

Lee, H.J., Saravanos, D.A., 1997. Generalized finite element formulation for smart multilayered thermal piezoelectric composite plates. Int. J. Solids Struct. 34, 3355–3371.

Lee, H.J., Saravanos, D.A., 2000. A mixed multi-field finite element formulation for thermopiezoelectric composite shells. Int. J. Solids Struct. 37, 4949–5967.

Nan, C.W., 1994. Magnetoelectric effect in composites of piezoelectric and piezomagnetic phases. Phys. Rev. B 50, 6082–6088.

Pagano, N.J., 1969. Exact solutions for composites in cylindrical bending. J. Compos. Mater. 3, 398–411.

Pagano, N.J., 1970. Exact solutions for rectangular bidirectional composites and sandwich plates. J. Compos. Mater. 4, 20–34.

Pan, E., 1991. An exact solution for transversely isotropic, simply supported and layered rectangular plates. J. Elasticity 25, 101–116.

Pan, E., 1997. Static Green's functions in multilayered half spaces. Appl. Math. Modelling 21, 509–521.

Pan, E., 2001. Exact solution for simply supported and multilayered magneto-electro-elastic plates. J. Appl. Mech. 68, 608–618.

Pan, E., Heyliger, P., 2002. Free vibrations of simply supported and multilayered magneto-electro-elastic plates. J. Sound Vib. 253, 429–443.

Stroh, A.N., 1958. Dislocations and cracks in anisotropic elasticity. Phil. Mag. 3, 625–646.

Timoshenko, S., Woinowsky-Krieger, S., 1987. Theory of Plates and Shells. McGraw-Hill, New York.

Ting, T.C.T., 1996. Anisotropic Elasticity. Oxford University Press, Oxford.

Tzou, H.S., 1993. Piezoelectric Shells, Distributed Sensing and Control of Continua. Kluwer Academic, Norwell, MA.

Tzou, H.S., Tseng, C.I., 1990. Distributed piezoelectric sensor/actuator design for dynamic measurement/control of distributed parametric systems: a piezoelectric finite element approach. J. Sound Vib. 138, 17–34.

Tzou, H.S., Ye, R., 1996. Analysis of piezoelastic structures with laminated piezoelectric triangle shell elements. AIAA J. 34, 110–115.

Vel, S.S., Batra, R.C., 2000. Three-dimensional analytical solution for hybrid multilayered piezoelectric plates. J. Appl. Mech. 67, 558–567.